Phase transitions in tungsten trioxide at high temperatures - a new look

1999 J. Phys.: Condens. Matter 11 6737

(http://iopscience.iop.org/0953-8984/11/35/312)

J. Phys.: Condens. Matter **11** (1999) 6737–6756. Printed in the UK PII: S0953-8984(99)02921-5

Phase transitions in tungsten trioxide at high temperatures—a new look

K R Locherer†, I P Swainson‡ and E K H Salje†

† Department of Earth Sciences, and IRC in Superconductivity, University of Cambridge, Cambridge CB2 3EQ, UK
‡ NPMR, SIMS, NRC, Chalk River Laboratories, Chalk River, ON, Canada KOJ 1J0

E-mail: ian.swainson@nrc.ca (I P Swainson) and es10002@esc.cam.ac.uk (E K H Salje)

Received 19 March 1999

Abstract. Neutron powder diffraction results on the tetragonal–orthorhombic and orthorhombic–monoclinic structural phase transitions of tungsten oxide are reported. The observed first-order transition from $P4/ncc$ to $Pnma$ at 980 K to 1200 K hides the transition from the higher-temperature phase $P4/nmm$ (via $Cmca$) to $Pnma$. At 623(24) K, $Pnma$ transforms via octahedral rotations in a tricritical transition to $P2_1/n$. The structural characteristics and thermodynamic properties of the order parameters are described in detail. The evolution of the WO_6 octahedra and the atomic positions is documented using such parameters as the octahedral elongation, octahedral variance and the off-centre displacement vectors for the tungsten atoms. It is shown that the phase transitions can be adequately described within the framework of a decoupled mean-field Landau theory.

1. Introduction

The structure of tungsten trioxide is perovskite-like, with corner-sharing WO_6 octahedra. Between absolute zero and 230 K the symmetry is monoclinic, with space group Pc [1–3]. At higher temperatures up to room temperature the structure is triclinic, $P\bar{1}$ [4,5]. Between room temperature and 600 K WO_3 is monoclinic, of symmetry $P2_1/n$ [6,7]. Up to near 1000 K its structure is $Pmnb$ ($Pnma$) [8]. Above this temperature the symmetry is $P4/ncc$ [9], and at 1170 K it becomes $P4/nmm$ [10]. The two tetragonal phases were reinvestigated by Locherer *et al* [9] using neutron diffraction techniques, because better data were needed to determine the order parameter.

The technological importance of WO_3 in the fields of electrochromics [11–13], superconductivity [14, 15] and nanotechnology [16] as well as the study of (bi)polarons [3, 17] makes this material one of the best researched transition metal oxides. Despite the great effort in the characterization of WO_3 a detailed determination of the structural properties of the phase transitions is still missing, mainly because much of the early work was undertaken using x-ray powder diffraction techniques. A recently discovered tetragonal modification of reduced WO_3 is believed to produce a phase which exhibits sheet superconductivity [14, 15], and has caused a resurgence of interest in the structural properties of WO_3. In this paper we report the detailed atomic motion of the atomic positions during phase transitions as determined by neutron diffraction methods.

0953-8984/99/356737+20$30.00

2. Experiments

Material for the powder diffraction experiments was obtained in two steps. A platinum crucible was filled with 99%+ pure WO_3 powder of 20 μm grain size (Aldrich, catalogue No 23278-5) and placed in a furnace at 1073 K for 100 hours [8]. The temperature was then raised to 1723 K for about two hours. The timescale at this point is critical, as WO_3 sublimates very rapidly at these temperatures, and if one leaves the material for too long nothing is left in the crucible. The furnace is then turned off and left to cool to room temperature. From the surface of the recrystallized mass, crystals with plate-like habit (parallel to 001) were recovered. These were then ground in acetone.

A series of neutron diffraction patterns were taken between room temperature and 1210 K at the C2 diffractometer at Chalk River Laboratories (see figures 1 and 2). The wavelength was $\lambda = 2.3717$ Å. The neutrons were filtered using pyrolytic graphite to reduce $\lambda/2$ contamination.

Lattice parameters were extracted using the Pawley method [18] in FULLPROF [19] (tables 1 and 2). The results for temperatures above 989 K are reported elsewhere [9].

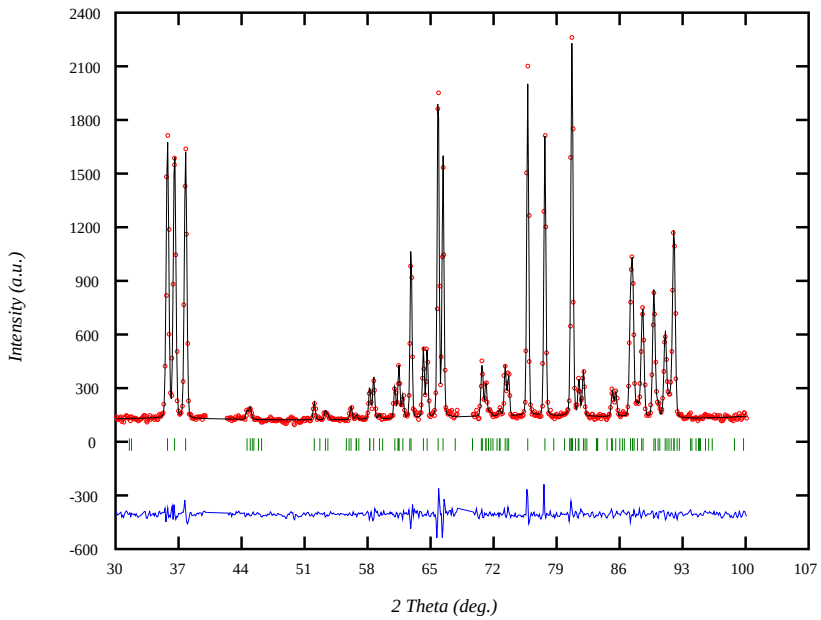

Figure 1. Observed, calculated and difference patterns of the monoclinic phase at 546 K. The reliability factors are $R = 4.55$, $R_{wp} = 6.01$ and $\chi^2 = 0.93$.

Table 1. The lattice parameters for the monoclinic phase at temperatures between 393(3) K and 653(3) K.

Temperature (K)	a (Å)	b (Å)	c (Å)	β
389(3)	7.3099(9)	7.5489(3)	7.7019(3)	90.827(3)
491(3)	7.3183(4)	7.5565(3)	7.7135(4)	90.721(4)
546(3)	7.3243(3)	7.5610(3)	7.7220(3)	90.638(3)
601(3)	7.3296(3)	7.5681(3)	7.7337(3)	90.459(3)
653(3)	7.3395(4)	7.5775(3)	7.7475(3)	90.059(7)

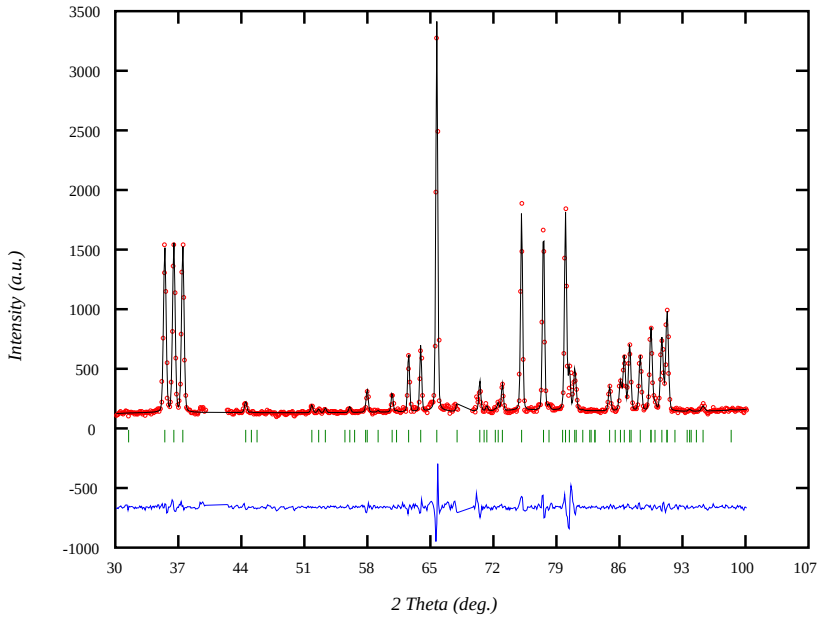

Figure 2. Observed, calculated and difference patterns of the orthorhombic phase at 908 K. The reliability factors are $R = 6.18$, $R_{wp} = 9.04$ and $\chi^2 = 2.06$.

Table 2. The lattice parameters refined for the orthorhombic phase at temperatures between 704(3) K and 989(3) K.

Temperature (K)	*a* (Å)	*b* (Å)	*c* (Å)
704(3)	7.3453(4)	7.5776(4)	7.7521(4)
755(3)	7.3519(4)	7.5778(4)	7.7573(4)
806(3)	7.3602(4)	7.5776(5)	7.7640(5)
857(3)	7.3691(4)	7.5765(4)	7.7717(4)
908(3)	7.3783(4)	7.5726(4)	7.7798(5)
918(3)	7.3801(5)	7.5720(5)	7.7819(5)
928(3)	7.3818(5)	7.5714(5)	7.7834(5)
939(3)	7.3840(5)	7.5703(5)	7.7862(6)
949(3)	7.3866(5)	7.5694(5)	7.7883(5)
959(3)	7.3889(5)	7.5685(5)	7.7904(5)
969(3)	7.3909(6)	7.5665(6)	7.7929(7)
979(3)	7.3935(4)	7.5651(5)	7.7956(5)
989(3)	7.3963(5)	7.5629(5)	7.7985(5)

3. The tetragonal–orthorhombic transition

3.1. The sub–supergroup relation

$Pnma$ is not a subgroup of $P4/ncc$. However, although $Pnma$ is not a maximal subgroup of $P4/nmm$ the two can be linked via an intermediate space group. This is illustrated in figures 3 and 4.

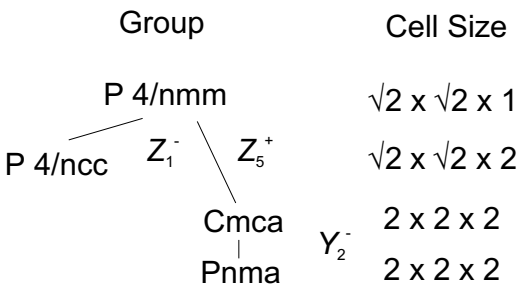

Figure 3. The super–subgroup relationships for the phases of WO_3. The definition of the special points is given in figure 4.

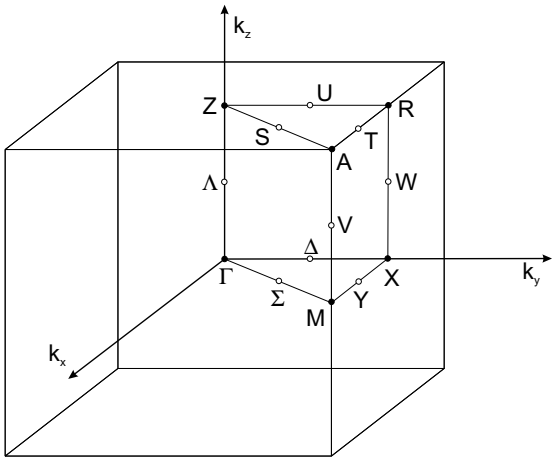

Figure 4. The Brillouin zone for tetragonal P: $\Gamma = (0, 0, 0)$, $M = (\frac{1}{2}, \frac{1}{2}, 0)$, $Z = (0, 0, \frac{1}{2})$, $A = (\frac{1}{2}, \frac{1}{2}, \frac{1}{2})$, $R = (0, \frac{1}{2}, \frac{1}{2})$, $X = (0, \frac{1}{2}, 0)$. The tetragonal–tetragonal transition $P4/nmm$ to $P4/ncc$ via $P4_2ncm$ correlates with the Z and Γ points respectively. The tetragonal–orthorhombic transitions $P4/nmm$ to $Cmca$ is also associated with the Z point. After Bradley and Cracknell [34].

The transition proceeds via the transformation matrix [20]

$$T_Z = \left[\begin{array}{ccc|c} 1 & 1 & 0 & 0 \\ \bar{1} & 1 & 0 & \frac{1}{2} \\ 0 & 0 & 2 & 0 \end{array}\right] \tag{1}$$

to $Cmca$ and then via

$$T_Y = \left[\begin{array}{ccc|c} 0 & 1 & 0 & \frac{1}{4} \\ 1 & 0 & 0 & \frac{1}{4} \\ 0 & 0 & \bar{1} & 0 \end{array}\right] \tag{2}$$

to $Pnma$. The splitting of the Wyckoff positions is recorded in table 3.

3.2. The spontaneous strain

The sequence shows that the transition between the tetragonal and orthorhombic phase in WO_3 does not take place between $P4/ncc$ and $Pnma$, but rather between $P4/nmm$ and $Pnma$, as

Table 3. Atomic coordinates and their correlations for the phases $P4/nmm$, $Cmca$ and $Pnma$. Atomic positions taken from Salje [8] and Locherer *et al* [9].

Super-group	Wyckoff position	Atom and coordinates				Sub-group	Wyckoff position	Atom (new label) and coordinates			
$P4/nmm$	2c	W^1	0.250	0.250	0.066	$Cmca$	8f	W^1	0.000	0.779	0.031
	2c	O^1	0.250	0.250	0.506		8f	O^1	0.000	0.754	0.262
	4d	O^2	0.000	0.000	0.000		8c	O^2	0.250	0.250	0.000
							4a	O^3	0.000	0.000	0.000
							4b	O^4	0.500	0.000	0.000
$Cmca$	8f	W^1	0.000	0.779	0.031	$Pnma$	4c	W^1	0.029	0.250	−0.031
							4c	W^2	0.030	0.250	0.468
	8f	O^1	0.000	0.754	0.262		4c	O^1	0.004	0.250	0.738
							4c	O^2	0.015	0.250	0.224
	8c	O^2	0.250	0.250	0.000		4a	O^3	0.000	0.000	0.000
							4b	O^4	0.000	0.000	0.500
	4a	O^3	0.000	0.000	0.000		4c	O^5	0.278	0.250	0.529
	4b	O^4	0.500	0.000	0.000		4c	O^6	0.269	0.250	−0.027

observed by Salje [8]. Instead of extrapolating the lattice parameters from the lower tetragonal phase into the orthorhombic phase to work out the strain the higher tetragonal phase has to be used. This is supported by the fact that the average lattice parameter in the orthorhombic phase $a_{ave} = (a_o + b_o)/2$ can be extrapolated to higher temperatures and can be made to virtually coincide with the a-axis parameter of $P4/nmm$ (figure 5).

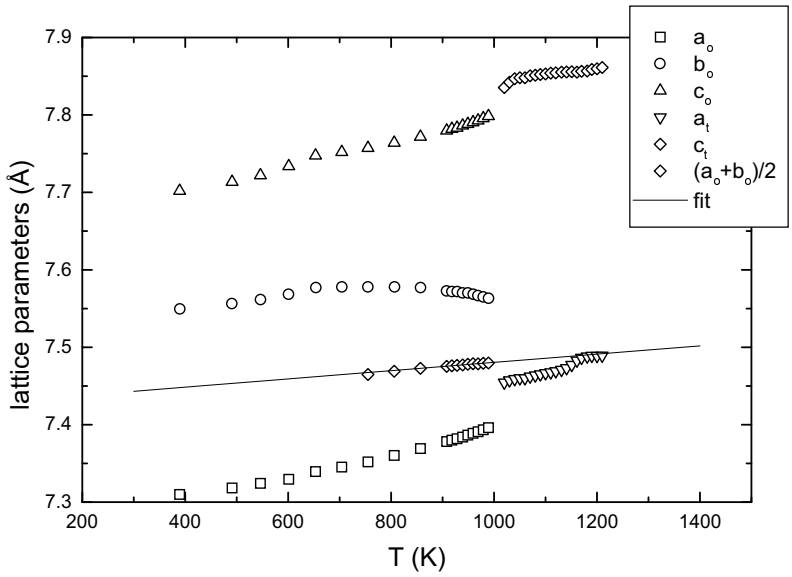

Figure 5. The lattice parameters extracted from neutron powder diffraction. The values above 989 K are reported in [9].

There is a small discrepancy between the extrapolations, which might be of significance. Linear fits to $a_{ave} = (a_o + b_o)/2$ give the relation $a_{ave} = [7.416(1) + 6.5(1) \times 10^{-5}\ \mathrm{K}^{-1}\ T]$ Å, while a linear fit to the tetragonal lattice parameters between 1170 K and 1210 K produces

$a_t = [7.411(2) + 6.4(1) \times 10^{-5}\ \mathrm{K}^{-1}\ T]$ Å. There is an offset between the fits of $a_{ave} - a_t \approx 0.005$ Å. This offset is larger than the error. It might be attributed to a non-symmetry-breaking transition somewhere between 980 K and 1170 K.

Ignoring the small discrepancy, either extrapolation can be used to obtain the orthorhombic spontaneous strains. The spontaneous strains e_{11} and e_{22} are nearly symmetrical about zero (figure 6), which implies that virtually all the strain relates to the symmetry-breaking spontaneous strain $(e_{11} - e_{22})/2$, whereas the non-symmetry-breaking spontaneous strain $(e_{11} + e_{22})/2$ is practically zero. Figure 7 shows a plot of e_{11} versus e_{22}. The two strains scale linearly.

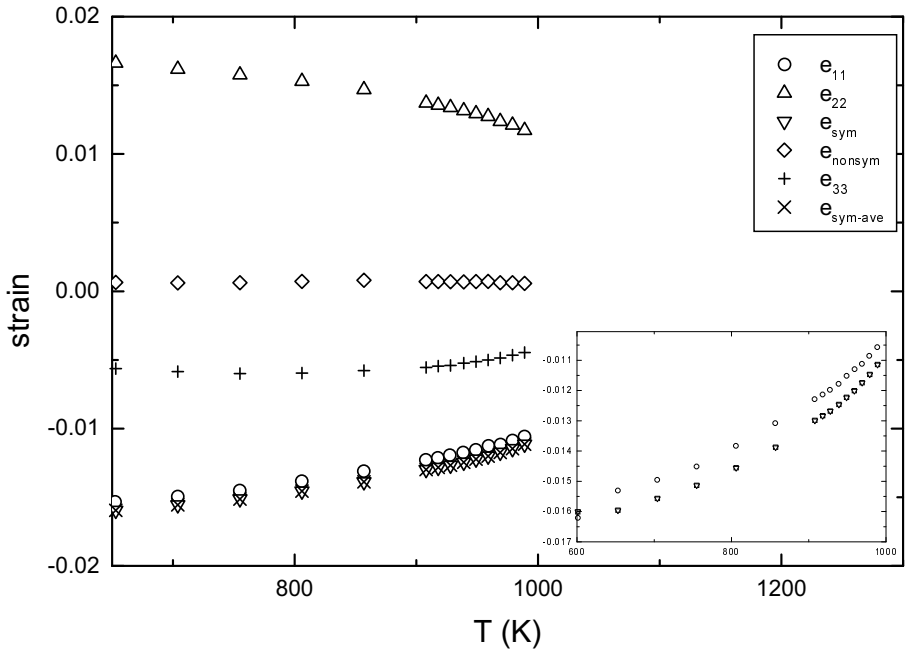

Figure 6. The various strains versus temperature for WO_3. The inset shows details of the strains e_{11}, e_{sym} and $e_{(a-b)/(a+b)}$. Errors are of the size of the plot symbols, except for e_{33} (see the text).

To obtain the *c*-axis spontaneous strain of the orthorhombic phase the tetragonal *c* lattice parameter was extrapolated to lower temperatures. As for the basal plane, only five data points could be used. The linear fit between 1170 K and 1210 K gave the result $c_t = [7.71(2) + 1.25(1) \times 10^{-4}\ \mathrm{K}^{-1}\ T]$ Å. The errors are very large. Hence the reliability of the derived strain is limited. The strain e_{33} is plotted in figure 6. It levels off towards lower temperatures and almost reverses its slope. This is likely to be caused by the error in the extrapolation of the lattice parameter.

Plotting e_{33} versus e_{sym} (figure 8) shows that the two strains scale linearly, which implies that the symmetry-breaking strain is proportional to the square of the order parameter. Closer examination reveals that the extrapolation in figure 8 does not pass through the origin. This point will be discussed further on.

An attempt was made to fit the strains using a Landau-type first-order 2–4–6 potential (see e.g. Salje [21]),

$$L(Q) = \frac{1}{2}A(T - T_c)Q^2 + \frac{1}{4}BQ^4 + \frac{1}{6}CQ^6. \tag{3}$$

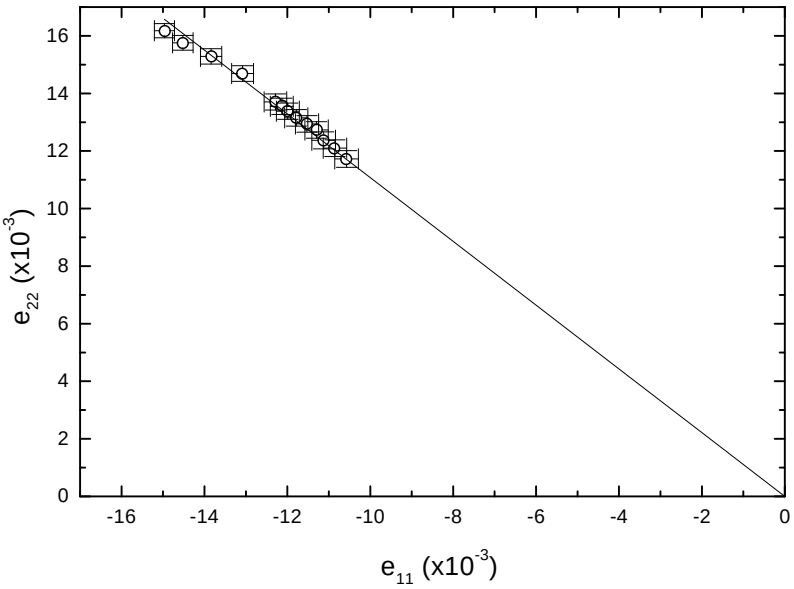

Figure 7. Linear correlation between e_{11} and e_{22}.

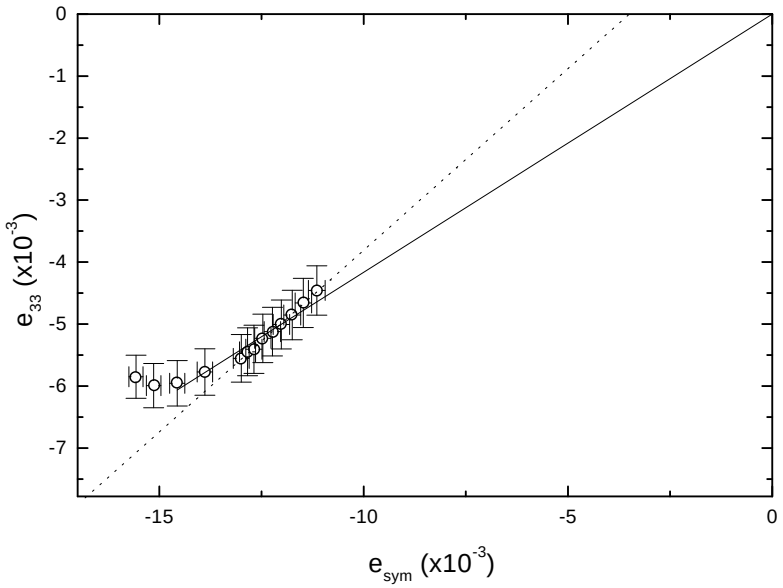

Figure 8. Correlation of e_{33} with the symmetry-breaking spontaneous strain e_{sym}. The solid line is a linear fit forced through the origin, while the dotted line is unconstrained.

The equilibrium transition temperature T_{Tr} is

$$T_{Tr} = T_c + \frac{3}{16}\frac{B^2}{AC}. \tag{4}$$

The order parameter jumps from $Q = 0$ to $Q = Q_0$ at T_{Tr}, where Q_0 is

$$Q_0 = \pm\left[-\frac{4A(T_{Tr} - T_c)}{B}\right]^{1/2}. \tag{5}$$

Below T_{Tr} the order parameter is described by

$$Q^2 = \frac{2}{3}Q_0^2\left\{1 + \left[1 - \frac{3}{4}\left(\frac{T - T_c}{T_{Tr} - T_c}\right)\right]^{1/2}\right\}. \tag{6}$$

The strain was linearized such that

$$y = \frac{4}{3}\left[1 - \left(\frac{3}{2}\frac{e_{sym}}{e_{sym,0}} - 1\right)^2\right] \tag{7}$$

$$x = T. \tag{8}$$

This is plotted in figure 9. Since e_0 has to be specified by choosing T_{tr} this opens up the possibility that the 'real' T_{tr} is covered up by the phase $P4/ncc$, rendering the linearization wrong. Nevertheless the transformed spontaneous strain scales linearly with temperature within error, supporting the chosen model. The linear fit $y = mx + c$ between 700 K and 989 K returns the parameters $c = -3.50(8)$ and $m = 4.51(9) \times 10^{-3}$ K^{-1} at a correlation factor of $R = 0.997$ and standard deviation of $\sigma = 0.25$. This leads to $T_c = -c/m = 780(21)$ K. In checking for self-consistency it is found that the fit gives $T_{tr} = (1 - c)/m = 995(31)$ K, which is close to the original input $T_{tr} = 989$ K. The same procedure was applied to a 2–3–4 potential,

$$L(Q) = \frac{1}{2}A(T - T_c)Q^2 + \frac{1}{3}BQ^3 + \frac{1}{4}CQ^4. \tag{9}$$

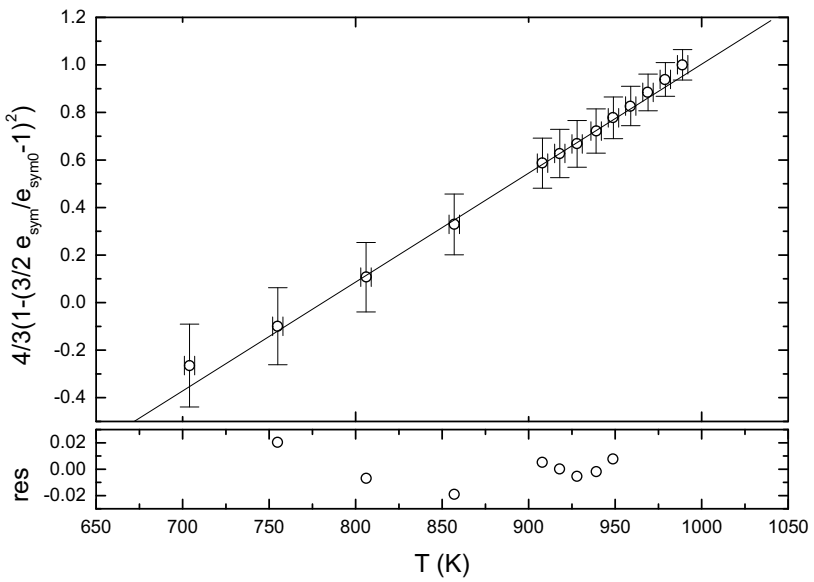

Figure 9. Temperature dependence of the linearized strain for a 2–4–6 potential. A plot of the residual of the fit is shown at the bottom of the graph.

This gives an equilibrium transition temperature of

$$T_{Tr} = T_c + \frac{2}{9}\frac{B^2}{AC}. \tag{10}$$

At T_{Tr} there will be a jump in the order parameter from $Q = 0$ to $Q = Q_0$, where

$$Q_0 = \pm\frac{2}{3}\frac{B}{C}. \tag{11}$$

For temperatures below T_{Tr} the variation of the order parameter is

$$Q = \frac{3}{4}Q_0\left\{1 + \left[1 - \frac{8}{9}\left(\frac{T - T_c}{T_{Tr} - T_c}\right)\right]^{1/2}\right\}. \tag{12}$$

Again, the strain data were linearized according to

$$y = \frac{9}{8}\left[1 - \left(\frac{4}{3}\frac{e_{sym}}{e_{sym,0}} - 1\right)^2\right] \tag{13}$$

$$x = T. \tag{14}$$

This is plotted in figure 10. A linear fit now produces the values $c = 0.10(3)$ and $m = 9.0(3) \times 10^{-4}$ K^{-1} at a correlation factor of $R = 0.992$ and a standard deviation of $\sigma = 0.57$. Statistically the fit is not as good as the first. It is particularly noticeable from the residual of the fit which shows a trend rather than equal scatter across zero. Hence this model was discarded.

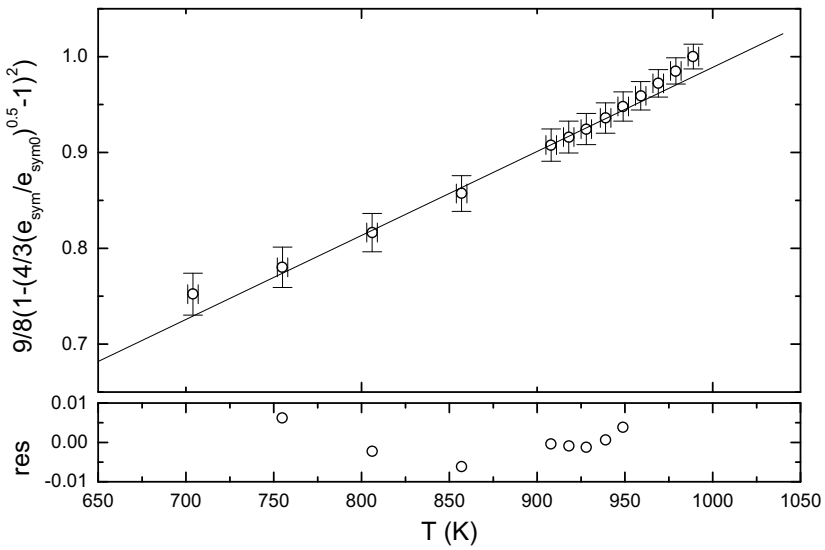

Figure 10. Temperature dependence of the linearized strain for a 2–3–4 potential. A plot of the residual of the fit is shown below at the bottom of the graph.

4. Discussion

4.1. The phenomenological model

In the previous section an attempt was made to fit the symmetry-breaking strain with a simple one-order-parameter model. This is inadequate. The transition will be influenced by other

phase transitions at higher temperatures. The hypothetical transition from the prototype $Pm\bar{3}m$ perovskite-type phase to $P4/nmm$ correlates with a soft mode at the M point of the Brillouin zone (figure 11) [8]. The transition causes a doubling of the unit cell according to [20]

$$T_M = \left[\begin{array}{ccc|c} 1 & 1 & 0 & \frac{1}{2} \\ \bar{1} & 1 & 0 & 0 \\ 0 & 0 & 1 & 0 \end{array}\right] \tag{15}$$

and produces a three-component order parameter. However, only one component is finite. This order parameter is associated with the puckering of the tungsten atoms in the basal plane. If the transition is continuous, as allowed by theory, the transition must be at a very high temperature, or may not occur at all, since the displacement of these atoms appears not to change significantly over the observed temperature range. This was also noted by Kehl *et al* [10] by considering the difference between the c- and the a-axis, which remains significant up to sublimation temperatures. Should the transition be of first order the transition temperature might be significantly reduced. In either case T_c appears to be at least as high as 1200 K. The order parameter, Q_1, can thus be taken as effectively constant with temperature over the range relevant to the lower WO_3 phases, and does not play a part in the lower-temperature transitions. That leaves two order parameters associated with the $P4/nmm$-to-$Cmca$ and the $Cmca$-to-$Pnma$ transitions, Q_2 and Q_3 respectively. To account for the observed behaviour, coupling between order parameters has to be taken into account. Salje and Devarajan [22] have discussed strain-induced order parameter coupling. The free energy becomes

$$\begin{aligned} G(Q_2, Q_3) &= \frac{1}{2}A_2Q_2^2 + \frac{1}{4}B_2Q_2^4 + \frac{1}{6}C_2Q_2^6 + \\ &= \frac{1}{2}A_3Q_3^2 + \frac{1}{4}B_3Q_3^4 + \frac{1}{6}C_3Q_3^6 + e_2Q_2^2 + e_3Q_3^2 + fe^2 \end{aligned} \tag{16}$$

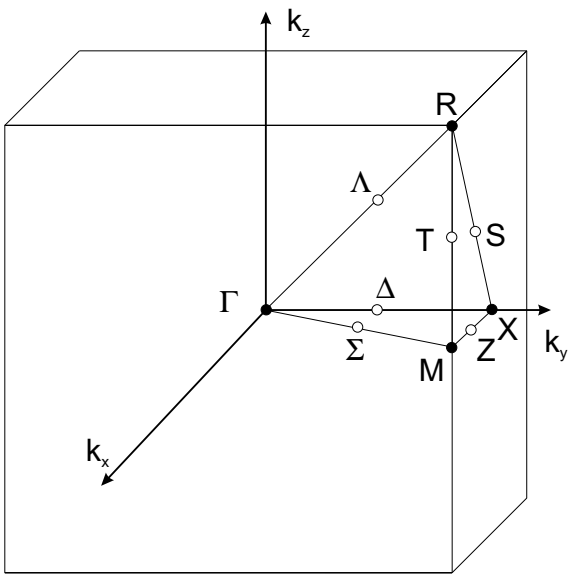

Figure 11. The Brillouin zone for cubic P: Γ(000), X = (0, $\frac{1}{2}$, 0), M = ($\frac{1}{2}$, $\frac{1}{2}$, 0), R = ($\frac{1}{2}$, $\frac{1}{2}$, $\frac{1}{2}$). The hypothetical transition from $Pm\bar{3}m$ to $P4/nmm$ is associated with the M point. After Bradley and Cracknell [34].

where both order parameters couple biquadratically to the strains. Minimization with respect to stress leads to

$$e = -\frac{d_2 Q_2^2 + d_3 Q_3^2}{2f}. \tag{17}$$

Thus the B-parameter in the Landau expression is renormalized such that

$$\begin{aligned} G = {} & \frac{1}{2}A_2 Q_2^2 + \frac{1}{4}\left(B_2 - \frac{e_2^2}{f}\right)Q_2^4 + \frac{1}{6}C_2 Q_2^6 \\ & + \frac{1}{2}A_3 Q_3^2 + \frac{1}{4}\left(B_3 - \frac{e_3^2}{f}\right)Q_3^4 + \frac{1}{6}C_3 Q_3^6 - \frac{e_2 e_3}{2f}Q_2^2 Q_3^2. \end{aligned} \tag{18}$$

Minimization of this equation with respect to the order parameters leads to the four solutions

$$\begin{aligned} &\text{O:} && Q_2 = Q_3 = 0 \\ &\text{I:} && Q_2 = 0,\ Q_3 = \frac{1}{2C_3}(-B_3 \pm (B_3^2 - 4A_3C_3)^{1/2}) \\ &\text{II:} && Q_3 = 0,\ Q_2 = \frac{1}{2C_2}(-B_2 \pm (B_2^2 - 4A_2C_2)^{1/2}) \\ &\text{III:} && Q_2 \neq 0,\ Q_3 \neq 0. \end{aligned} \tag{19}$$

This introduces seven unique topologies for the order parameters, depending on the various constants in the free-energy expansion, as discussed in Salje and Devarajan [22]. The observed sequence in this study is O–O′–II–III, where O′ represents the phase with $Q_1 \neq 0$. The paraelastic phase with all order parameters at zero changes in the $Pm\bar{3}m$-to-$P4/nmm$ transition to a phase with $Q_1 \neq 0$ (O′). At a lower temperature the phase becomes a mixture of all three order parameters through the transition to $Cmca$, with both $Q_1 \neq 0$ and $Q_2 \neq 0$. Finally, the transition to $Pnma$ creates a phase where all three order parameters are finite, $Q_1, Q_2, Q_3 \neq 0$. The observation of this particular sequence suggests that the coupling between all the order parameters is small [22], which explains why a decoupled order parameter model can successfully be applied in this study.

4.2. The microscopic transition mechanism

The change from $P4/nmm$ to $Cmca$ proceeds through a soft mode at the Z point of the Brillouin zone (figure 12). The order parameter Q_2 correlates with a zigzag displacement of the tungsten atoms along [100] in the basal plane of the orthorhombic cell, away from the centre of the octahedra (figure 13). The displacement is in opposite directions for layers parallel to (001) at $z = 0$ and $z = 0.5$, causing the doubling of the unit cell in c. In addition, there is a displacement of the apex oxygens along the same directions. This does not lead to a tilt of the octahedra, since the basal oxygens do not move. It is thus a further distortion of the octahedra. The magnitude of the displacement of the atoms is not known since the phase is not observed. However, the fractional coordinates of the orthorhombic phase $Pnma$ were used to construct the hypothetical structure. Using this hypothetical structure the magnitude of the displacement of the tungsten atoms is similar to the puckering in the tetragonal phase. While the displacement is $z/2c = 0.033$ in $P4/nmm$, it is $x/a = 0.029$ in $Cmca$. The oxygens move by only a very small amount, $x/a = 0.004$ (the standard deviation of the oxygen positions is 0.01; cf. Salje [8]). The combination of the tungsten and oxygen movements change the bond angle between the apex oxygens and the tungsten from 180° to 167°.

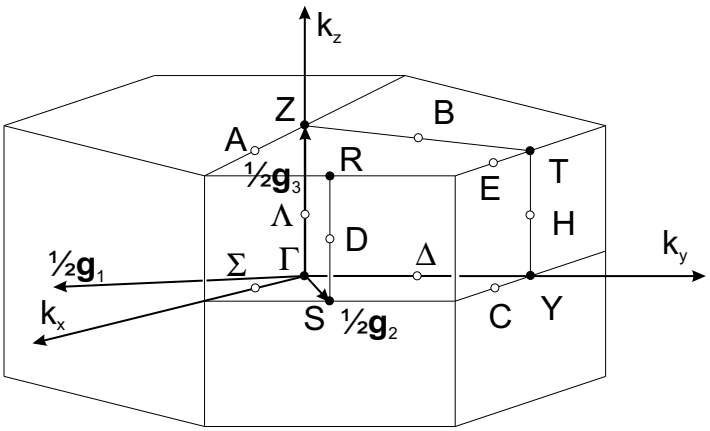

Figure 12. The Brillouin zone for orthorhombic C ($b > a$): $\Gamma = (0, 0, 0)$, $Y = (-\frac{1}{2}, \frac{1}{2}, 0)$, $Z = (0, 0, \frac{1}{2})$, $T = (-\frac{1}{2}, \frac{1}{2}, \frac{1}{2})$, $S = (0, \frac{1}{2}, 0)$, $R = (0, \frac{1}{2}, \frac{1}{2})$. The orthorhombic–orthorhombic transition *Cmca* to *Pnma* is associated with the Y point. After Bradley and Cracknell [34].

A measure of the distortion of the octahedra is given by the mean octahedral elongation and the octahedral angle variance [23]

$$\langle \lambda_{oct} \rangle = \frac{1}{6} \sum_{i=0}^{6} (l_i / l_0)^2 \tag{20}$$

$$\sigma_{oct}^2 = \frac{1}{11} \sum_{i=0}^{12} (\theta_i - 90^\circ)^2 \tag{21}$$

where l_i are the centre-to-apex distances and θ_i are the octahedral angles of the strained octahedron, while l_0 is the centre-to-apex distance in a perfect octahedron. Thus here the octahedral elongation corresponds to $\langle \lambda_{oct} \rangle = 1.027$, while the octahedral angle variance is $\sigma_{oct} = 8.43^\circ$. This re-emphasizes that the distortion of the octahedra has increased significantly. The symmetry of the octahedra changes from $4/mmm$ to 1.

The transition from *Cmca* to *Pnma* is associated with the Y point of the Brillouin zone (figure 12) and is non-ferroic, as there is no change in the point group. The order parameter Q_3 causes additional puckering in the basal plane. There are three processes associated with this transition. Firstly, the puckering of the tungsten atoms in the planes parallel to (100) at $x = 0.25$ and $x = 0.75$ of *Cmca* changes (figure 13). While the displacements of the atoms along [100] were previously out of phase for consecutive layers of planes, these now become in phase, albeit with slightly different magnitudes. This destroys the screw diads parallel to [001] at $(\frac{1}{4}, 0)$. Secondly, the basal oxygen atoms, which lie on the special position $(\frac{1}{4}, \frac{1}{4}, 0)$ are distorted in the same directions as the neighbouring tungstens in [100]. Thirdly, the oxygens in the planes parallel to (001) at $z = 0.25$ and $z = 0.75$ were previously aligned in the same directions within the same plane. A further distortion of the oxygens completes puckering of the (020) planes. The magnitude of the distortion for the tungsten atoms is $x/a = 0.029$ and $x/a = 0.030$. The oxygens in the (004) planes are displaced by $x/a = 0.004$ and $x/a = 0.015$, while in the basal plane it is $x/a = 0.028$ and $x/a = 0.019$. Again the transition does not produce a rotation of octahedra. The octahedral elongation is $\langle \lambda_{oct} \rangle = 1.014$ and $\langle \lambda_{oct} \rangle = 1.036$, the octahedral variance $\sigma = 6.63^\circ$ and $\sigma = 10.68^\circ$, while the octahedral volumes are $V = 8.57$ Å^3 and $V = 9.49$ Å^3. The bond length variance has increased to $\sigma_{bond} = 0.06$ Å and $\sigma_{bond} = 0.10$ Å respectively. Thus the distortion of one octahedron has decreased at the expense of the other.

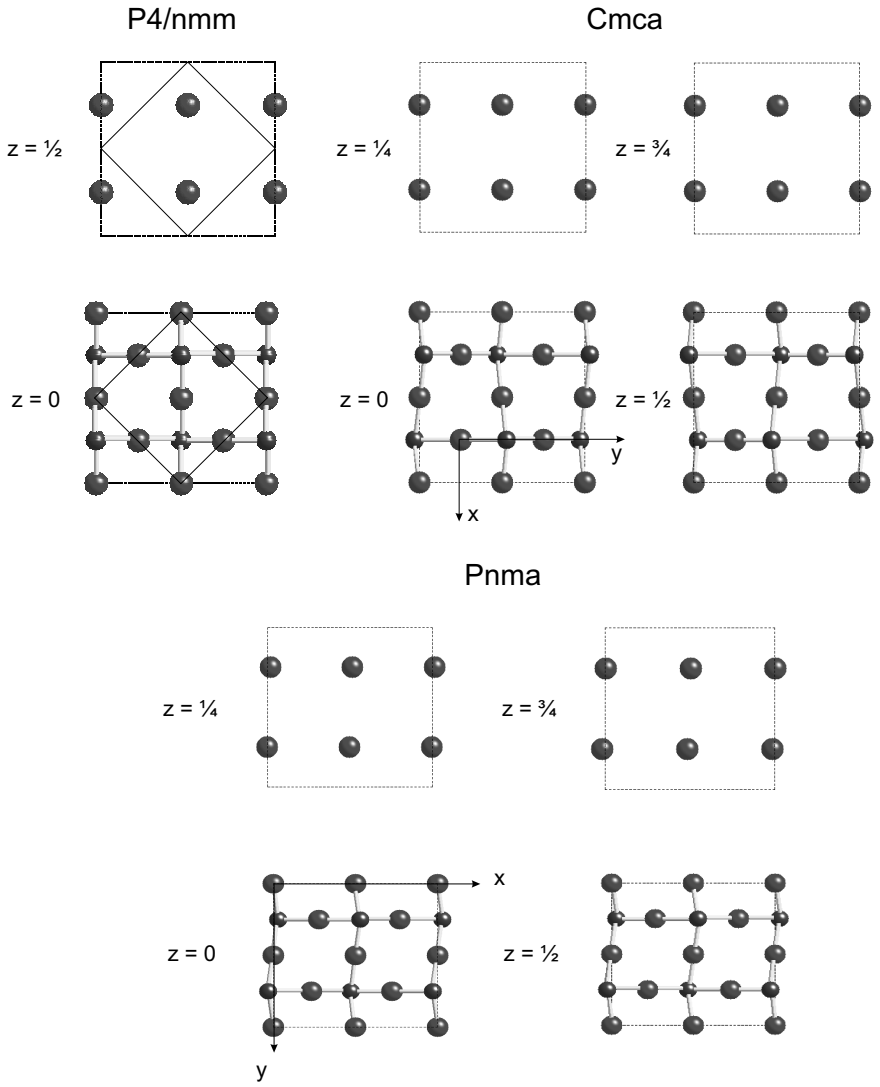

Figure 13. The structural characteristics of three phases of WO_3 are shown within the unit cell of the *Pnma* phase. The smaller spheres represent the tungsten atoms. The $P4/nmm$ phase (top left) contains a smaller unit cell indicated by the full line. The coordinate system shown for the $z = 0$ layer of the $Cmca$ phase shows the location of the origin of its unit cell. The puckering in the (001) plane is preserved throughout the transition. On the other hand the transformation produces additional puckering of similar magnitude in the (010) plane.

5. The monoclinic–orthorhombic transition

The monoclinic phase of WO_3 was first refined by Tanisaki [6] using x-ray single-crystal diffraction. The space group was given as $P2_1/n$, with lattice parameters $a = 7.30$ Å, $b = 7.53$ Å, $c = 7.68$ Å and $\beta = 90.9^\circ$. Further improvements on the refinement were achieved by Loopstra and Boldrini [7] and Loopstra and Rietveld [24] using neutron powder diffraction. The most recent refinement was done by Woodward *et al* [5] for a mixture of

triclinic and monoclinic WO_3, which led to minor changes of the structure. The transition between the orthorhombic and monoclinic transition was classified continuous by Salje and Viswanathan [25]. However, Brækken [26] comments that the monoclinic angle evolves continuously up to near the transition and then shows a small discontinuity.

The variation of the angle between monoclinic domains, i.e. the angle of spontaneous rotation, was first measured by Sawada and Danielson [27] using an optical microscope. The tensor of the spontaneous strain for the orthorhombic to monoclinic transition is given by

$$e_{sp} = \begin{bmatrix} 0 & 0 & e \\ 0 & 0 & 0 \\ e & 0 & 0 \end{bmatrix}. \tag{22}$$

The strain is equal to the angle of spontaneous rotation. Since there is no doubling of the unit cell in the transition it must be zone centred. Thus the strain is expected to be proportional to the order parameter. The strain in an orthorhombic-to-monoclinic transition is given by

$$e_{13} \propto \cos\beta. \tag{23}$$

On the assumption that the monoclinic angle is half the spontaneous rotation plus 90°, $\beta = \theta_{mono}/2 + 90$, a linear fit of

$$e_{13}^2 \propto Q^2 = Q_0^2(T_c - T) \tag{24}$$

was attempted. However, a better fit was achieved if the fourth power of the strain was used instead. The fit parameters then give a transition temperature of $T_c = 600(28)$ K (figure 14).

The variation of the monoclinic angle was also measured by Salje and Viswanathan [25] using powder x-ray diffraction. The resulting strain is plotted in figure 15. Again, fitting the fourth power of the strain produces a good fit, and gives the transition temperature $T_c = 712(72)$ K.

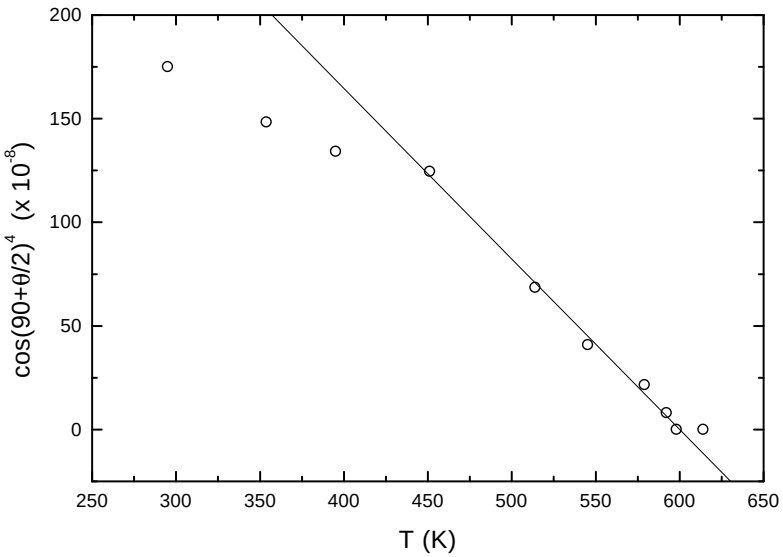

Figure 14. The fourth power of the cosine of 90° plus half the optical extinction angle between two monoclinic domains. Data from Sawada and Danielson [27].

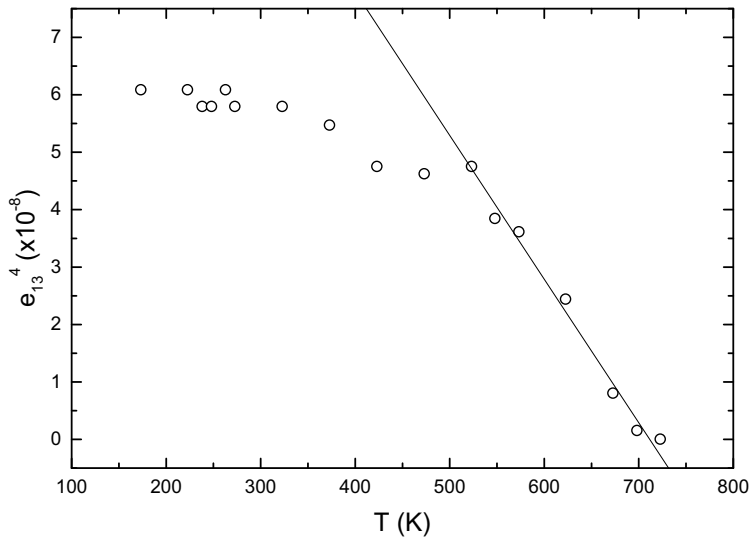

Figure 15. The fourth power of the cosine of the monoclinic angle versus temperature. Data taken from Salje and Viswanathan [25].

The temperature dependence of the order parameter can be modelled within the framework of Landau theory if the fourth-order term in the free-energy expansion is set to zero [21]:

$$L(Q) = \frac{1}{2}A(T - T_c)Q^2 + \frac{1}{6}CQ^6. \tag{25}$$

Below T_c the order parameter is

$$Q = \left[\frac{A}{C}(T_c - T)\right]^{1/4}. \tag{26}$$

Both data sets suggest that the transition is not second order but rather tricritical, while Brækken's [26] observation of a slight discontinuity suggests that the transition might be weakly first order.

When comparing the values for the monoclinic angles directly between the two publications two main discrepancies become apparent. Firstly, the transition temperature differs by over a hundred degrees. Secondly, the magnitudes of the monoclinic angle disagree.

From the variation of the monoclinic angle β refined in this study the strain was evaluated. Fitting the fourth power of the spontaneous strain gives $T_c = 623(24)$ K (figure 16). This seems to suggest that the transition temperature derived from the Sawada and Danielson [27] data is correct within error.

This study also reconfirms that the transition is tricritical. The magnitude of the monoclinic angle agrees with the Salje and Viswanathan [25] data (see table 1).

6. Discussion

The transition proceeds via the Γ point of the Brillouin zone (figure 17) [20]. Specific heat measurements reconfirm that the transition is tricritical [28].

In the monoclinic phase all the atoms lie on the [4e] general positions. The transition from

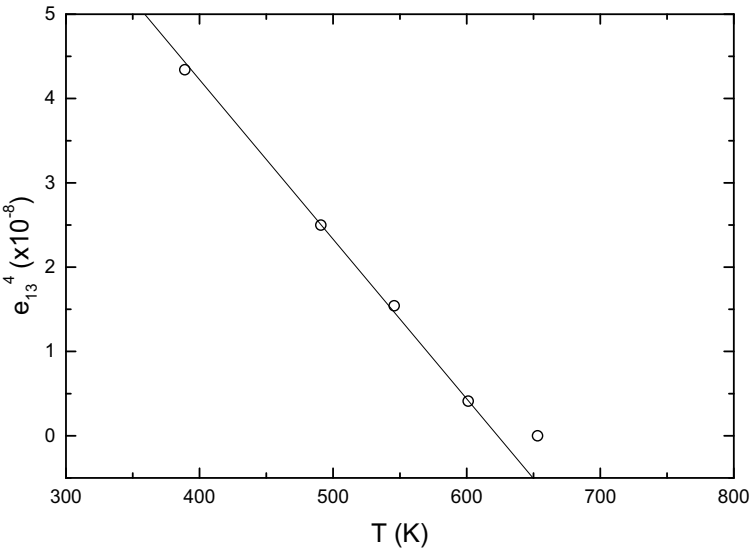

Figure 16. The fourth power of the monoclinic strain e_{13} versus temperature for the orthorhombic-to-monoclinic transition in WO_3. Errors are the size of the plot symbols.

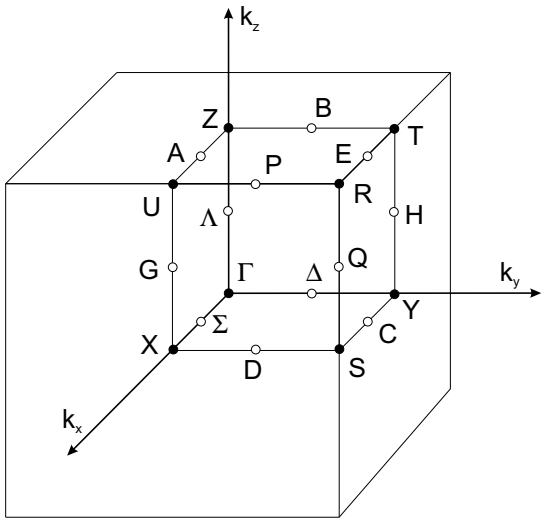

Figure 17. The Brillouin zone for orthorhombic P: $\Gamma = (0, 0, 0)$, $Y = (\bar{\frac{1}{2}}, 0, 0)$, $X = (0, \frac{1}{2}, 0)$, $Z = (0, 0, \frac{1}{2})$, $U = (0, \frac{1}{2}, \frac{1}{2})$, $T = (\bar{\frac{1}{2}}, 0, \frac{1}{2})$, $S = (\bar{\frac{1}{2}}, \frac{1}{2}, 0)$, $R = (\bar{\frac{1}{2}}, \frac{1}{2}, \frac{1}{2})$. The critical point for the *Pnma*-to-$P2_1/n$ transition is Γ. After Bradley and Cracknell [34].

Pnma to $P2_1/c$ is given by the matrix [20]

$$T_\Gamma = \left[\begin{array}{ccc|c} 0 & 1 & 0 & 0 \\ 0 & 0 & 1 & 0 \\ 1 & 0 & 0 & 0 \end{array}\right]. \tag{27}$$

To move up to *Pnma* two tungsten and four oxygen positions change to the special position [4c]. Thus the x-coordinate becomes $\frac{1}{4}$. The remaining two oxygen positions change to the special positions [4a] and [4b].

The monoclinic structure has been discussed by Woodward *et al* [5] in terms of octahedral tilting. Consider a pseudocubic subcell with parameters $a_p \neq b_p \neq c_p, \alpha \neq 90^\circ$. According

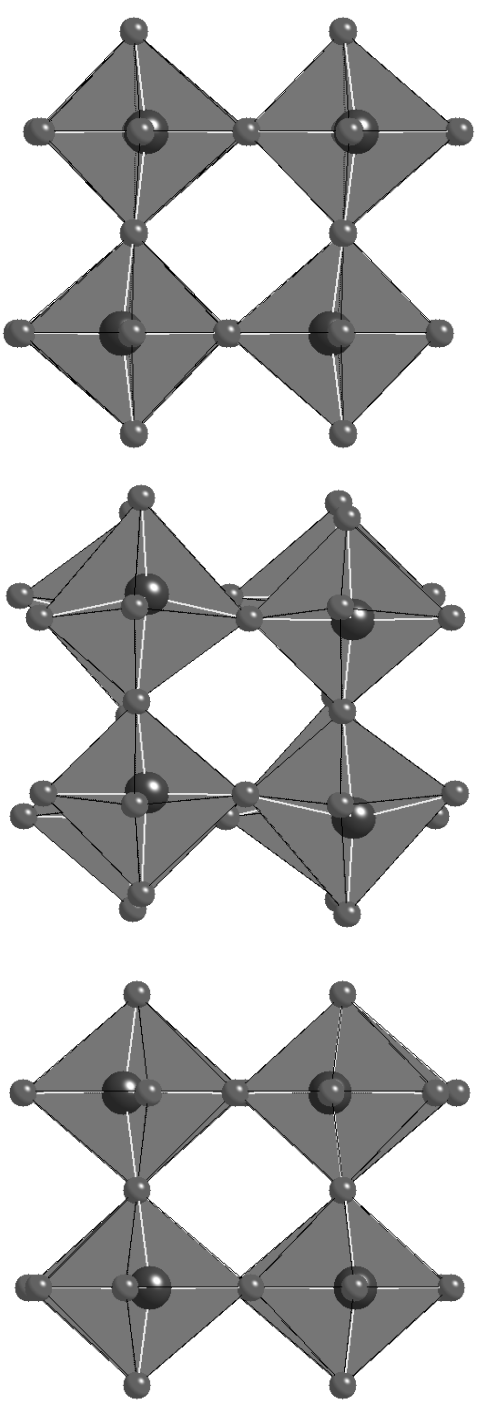

Figure 18. The crystal structure of the *Pnma* orthorhombic phase. The projection planes are from top to bottom: (001), (010) and (100).

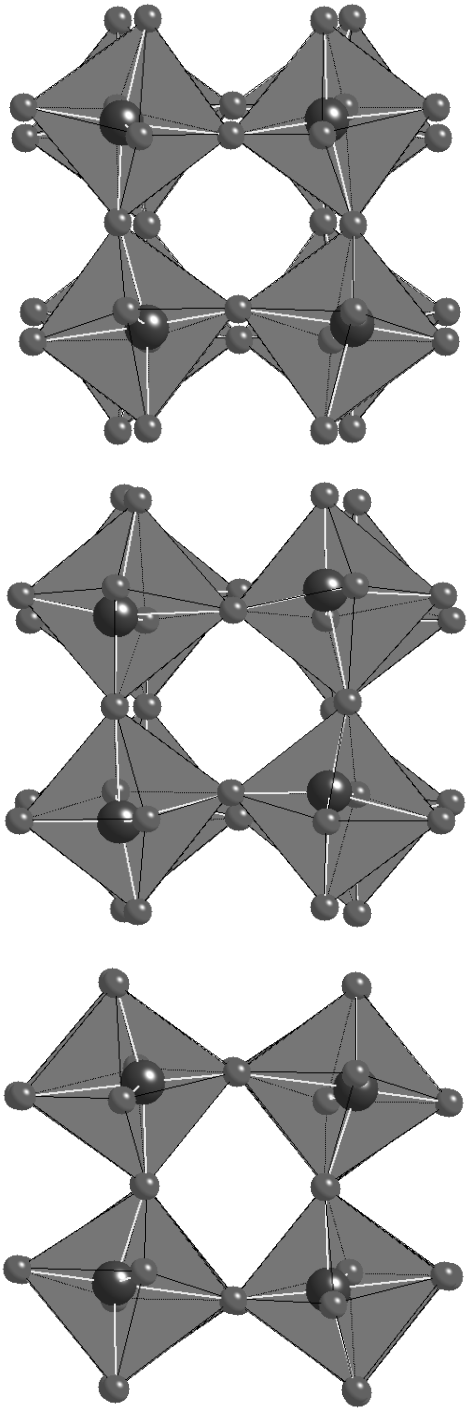

Figure 19. The crystal structure of the $P2_1/n$ monoclinic phase. The projection planes are from top to bottom: (001), (010) and (100).

to Glazer [29], the simple octahedral tilts $a^+b^-c^-$ lead to the structure for the corresponding monoclinic cell $2a_p \times 2b_p \times 2c_p$ of $A2_1/m$, or $P2_1/m$. However, this does not take into account the displacements of the tungsten atoms off the centre of the octahedra. If these are included in the analysis the mirror in $P2_1/m$ becomes the glide plane in $P2_1/n$. Thus the observed structure is reproduced if both the octahedral tilting and the tungsten displacements are taken into consideration. The orthorhombic and monoclinic structures are compared in figures 18 and 19.

The orthorhombic structure is a result of severe distortions of the octahedra. The monoclinic phase however has more regular octahedra. The octahedral elongation is $\langle\lambda_{oct}\rangle = 1.028$ and $\langle\lambda_{oct}\rangle = 1.027$ and the octahedral variance is $\sigma_{oct} = 8.60^\circ$ and $\sigma_{oct} = 8.31^\circ$. The volumes are $V = 9.34$ Å^3 and $V = 9.26$ Å^3. The similarity of the octahedral variance for the two octahedra in the monoclinic phase attests to the relaxation of the structure.

7. Conclusions

WO_3 displays a wide range of phase transitions. Various distortion parameters are summarized in table 4 for all known phases of WO_3. The phase with the highest symmetry is $P4/nmm$. This phase can be described by a soft mode at the M point of the $Pm\bar{3}m$ Brillouin zone [8]. It

Table 4. The octahedral elongation and variance for the various phases of WO_3. Also given are the volume of the WO_6 octahedra V_B and the cuboctahedral volume of the MO_{12} polyhedra V_A, where M is not occupied. The data were calculated using the following sources: (a) Locherer *et al* [9], (b) Aird *et al* [14], (c) Salje [8], (d) Loopstra and Rietveld [24], (e) Diehl *et al* [4], (f) Woodward and Sleight [2], The octahedral elongation and variance were calculated using the code VOLCAL [30]. The cuboctahedral volume was found using the relation $V_{unit\,cell} = Z(V_A + V_B)$ [31]. The octahedral volume, tungsten displacement vector and its magnitude were calculated using the code IVTON [32, 33].

Phase	$\langle\lambda_{oct}\rangle$	σ_{oct} (deg)	V_B (Å^3)	V_A (Å^3)	V_A/V_B	Tungsten displacement vector (fraction) and magnitude (Å)	
$P4/nmm$[a]	1.0190	6.82	9.220	46.102	5.0000	(0.0000, 0.0000, −0.0649)	0.255
$P4/ncc$[a]	1.0186	6.78	9.127	45.841	5.0227	(0.0000, 0.0000, 0.0318)	0.250
$P\bar{4}2_1m$[b]	1.0607	13.49	8.586	44.388	5.1700	(0.0018, 0.0018, −0.0675)	0.262
$Cmca$[a]	1.0273	8.41	9.088	54.531	6.0003	(0.0000, 0.0290, 0.0270)	0.304
$Pnma$[c]	1.0138	6.66	8.568	45.295	5.2863	(0.0180, 0.0000, 0.0153)	0.181
	1.0356	10.67	9.395	44.468	4.7329	(0.0190, 0.0000, 0.0350)	0.307
$P2_1/c$[d]	1.0282	8.59	9.333	43.627	4.6745	(−0.0390, 0.0199, −0.0039)	0.311
	1.0274	8.28	9.266	43.694	4.7155	(−0.0229, 0.0291, 0.0051)	0.310
$P\bar{1}$[e]	1.0253	7.75	9.265	43.476	4.6924	(0.0055, 0.0179, 0.0328)	0.290
	1.0284	8.56	9.428	43.313	4.5941	(−0.0037, 0.0198, −0.0355)	0.309
	1.0279	8.54	9.332	43.410	4.6520	(−0.0075, 0.0240, 0.0316)	0.311
	1.0244	7.96	9.149	43.592	4.7645	(0.0002, 0.0262, −0.0274)	0.285
P_c[f]	1.0234	7.77	9.342	42.771	4.5784	(0.0074, −0.0287, 0.0317)	0.286
	1.0292	8.72	9.286	42.826	4.6117	(−0.0029, −0.0147, −0.0405)	0.319

causes antiferroelectric displacements of the tungsten atoms in ⟨001⟩ directions, doubling the unit cell to $\sqrt{2} \times \sqrt{2} \times 1$ of the lattice parameters of the parent phase. This transition generates the first order parameter, which can be taken as constant within the observed temperature range. Furthermore a tricritical non-ferroic transition takes place to the $P4/ncc$ phase near 1171 K, which is caused by a soft mode at the Z point of the Brillouin zone [9]. The transition produces octahedral rotations described by a single tilt system $a^0a^0c^-$. The unit cell is doubled to $\sqrt{2} \times \sqrt{2} \times 2$. Near 1020 K a transition to orthorhombic symmetry $Pnma$ takes place. However, the transition does not proceed from $P4/ncc$. Instead $P4/nmm$ transforms to the intermediate phase $Cmca$ through a Z-point improper ferroelastic transition. A further order parameter appears, describing the zigzag displacements of tungstens along [100]. The unit cell has now the size $2 \times 2 \times 2$. $Cmca$ then transforms to $Pnma$ through a Y-point non-ferroic transition, which affects the positions of both tungsten and oxygen atoms. Figure 20 shows a hypothetical diagram of the high-temperature phases.

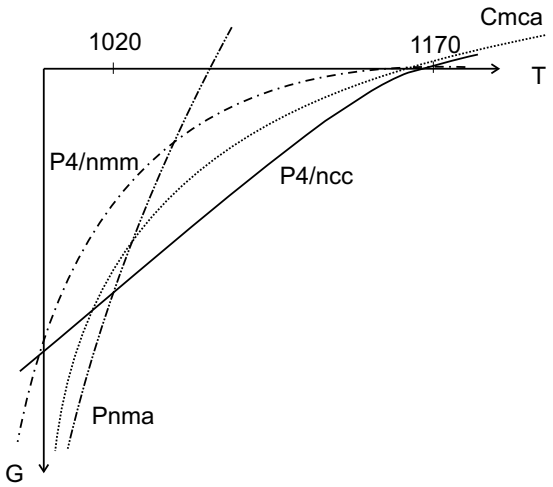

Figure 20. The hypothetical phase diagram for the higher-temperature phases of WO_3. The transition proceeds along the curve of lowest Gibbs free energy with the phases $P4/nmm$, $P4/ncc$ and $Pnma$.

Although the presence of three order parameters calls for a model with multiple order parameters it was found that one order parameter is enough to model the strain. A further transition takes place between $Pnma$ and $P2_1/n$. This tricritical proper ferroelastic transition is characterized by a soft mode at the Γ point of the Brillouin zone [8]. The mode causes tilting of the coordination octahedra. The transition temperature was found to be near 623 K. Again the transition is well described by a single order parameter.

Acknowledgments

The authors thank Ron Donaberger and Michael Watson for help with the experimental equipment at Chalk River. KRL would like to thank Magdalene College, Cambridge, and the EPSRC for financial support. Further assistance was provided by the European Community, the National Research Council of Canada and the Department of Earth Sciences, Cambridge.

References

[1] Salje E 1976 *Ferroelectrics* **12** 215
[2] Woodward P and Sleight A 1997 *J. Solid State Chem.* **131** 9
[3] Salje E K H, Rehmann S, Pobell F, Morris D, Knight K S, Herrmannsdörfer T and Dove M T 1997 *J. Phys.: Condens. Matter* **9** 6563
[4] Diehl R, Brandt G and Salje E 1978 *Acta Crystallogr.* B **34** 1105
[5] Woodward P, Sleight A and Vogt T 1995 *J. Phys. Chem. Solids* **56** 1305
[6] Tanisaki S 1960 *J. Phys. Soc. Japan* **15** 573
[7] Loopstra B and Boldrini P 1966 *Acta Crystallogr.* **21** 158
[8] Salje E 1977 *Acta Crystallogr.* B **33** 574
[9] Locherer K, Swainson I and Salje E 1999 *J. Phys.: Condens. Matter* **11** 4143
[10] Kehl W, Hay R and Wahl D 1952 *J. Appl. Phys.* **23** 212
[11] Granqvist C 1992 *Solid State Ion.* **53–56** 479
[12] Granqvist C 1994 *Solar Energy Mater. Solar Cells* **32** 369
[13] Pham Thi M and Velasco G 1985 *Revue Chim. Minérale* **22** 195
[14] Aird A, Domeneghetti M, Mazzi F, Tazzoli V and Salje E 1998 *J. Phys.: Condens. Matter* **10** 569
[15] Aird A and Salje E 1998 *J. Phys.: Condens. Matter* **10** 377
[16] Salje E, Aird A, Locherer K, Hayward S, Novak J and Chrosch J 1998 *Ferroelectrics* submitted
[17] Salje E 1994 *Eur. J. Solid State Inorg. Chem.* **31** 805
[18] Pawley G 1981 *J. Appl. Crystallogr.* **14** 357
[19] Rodriquez-Carvajal J 1993 *FULLPROF* Institut Laue–Langevin, Laboratoire Leon Brillouin (CEA-CNRS), Grenoble
[20] Stokes H and Hatch D 1988 *Isotropy Subgroups of the 230 Crystallographic Space Groups* 1st edn (Singapore: World Scientific)
[21] Salje E 1990 *Phase Transitions in Ferroelastic and Co-Elastic Crystals* (Cambridge: Cambridge University Press)
[22] Salje E and Devarajan V 1986 *Phase Transitions* **6** 235
[23] Robinson K, Gibbs G and Ribbe P 1971 *Nature* **172** 567
[24] Loopstra B and Rietveld H 1969 *Acta Crystallogr.* B **25** 1420
[25] Salje E and Viswanathan K 1975 *Acta Crystallogr.* A **31** 356
[26] Brækken H 1969 *K. Nor. Vidensk. Selsk. Foerhandl.* **42** 25
[27] Sawada S and Danielson G 1959 *Phys. Rev.* **113** 1005
[28] Sawada S 1956 *J. Phys. Soc. Japan* **11** 1246
[29] Glazer A 1972 *Acta Crystallogr.* B **28** 3384
[30] Finger L 1979 *VOLCAL—Program to Calculate Polyhedral Volumes and Distortion Parameters* Carnegie Institution of Washington, Washington, DC
[31] Thomas N 1996 *Acta Crystallogr.* B **52** 16
[32] Balic Zunic T and Vickovic I 1996 *Acta Crystallogr.* B **52** 78
[33] Balic Zunic T and Vickovic I 1996 *J. Appl. Crystallogr.* **29** 305
[34] Bradley C J and Cracknell A P 1972 *The Mathematical Theory of Symmetry in Solids* (Oxford: Oxford University Press)